

## SEISMIC PERFORMANCE OF A CONCRETE FACED ROCKFILL DAM USING AN ADVANCED NONLINEAR 3D NUMERICAL ANALYSIS

P. Dakoulas<sup>1</sup> and V. Evangelou<sup>2</sup>

<sup>1</sup> Associate Professor, Dept. of Civil Engineering, University of Thessaly, Volos, Greece

<sup>2</sup> Graduate Student, Dept. of Civil Engineering, University of Thessaly, Volos, Greece

Email: [dakoulas@uth.gr](mailto:dakoulas@uth.gr)

### ABSTRACT :

A general methodology is presented for advanced nonlinear 3D dynamic finite element analysis of concrete faced rockfill dams and applied to a dam build in a narrow canyon. Initially a detailed simulation of the phased construction and reservoir impoundment is conducted, using the Duncan and Chang (1970) constitutive model. After calculation of the initial stresses and deformations at the end of impoundment, the dynamic analysis is initiated using a nonlinear hysteretic model that is based on the initial dynamic stiffness of the rockfill material. The model produces hysteresis loops that are in agreement with the experimental data regarding the variation of the shear modulus and damping ratio with the amplitude of cyclic shear strain. The methodology is applied here to investigate the effect of (a) rockfill dynamic stiffness and (b) the possible development of seismic settlements on the seismic the response of the dam and the performance of the concrete slab and joints. Results are presented on the development of (a) tensile stresses at various locations within the concrete slab panels (b) joint separations due to movement of the slab panels and (c) high compressive stresses at the slab-to-slab vertical interfaces that may potentially lead to concrete fracture.

### KEYWORDS:

Rockfill Dams, CFRD, 3D Geometry, Nonlinear Analysis, Hysteretic Damping, Dynamic Settlements

### 1. INTRODUCTION

Due to the high shear strength of the compacted rockfill and the lack of water pressures, the concrete faced rockfill dams (CFRDs) are considered to behave better during earthquakes compared to conventional rockfill dams with an earth core (Wieland 2007, Gazetas & Dakoulas 1992, Sherard & Cooke 1987). However, this assessment is based on a very limited number of case histories of such dams. The strong earthquake ( $M = 7.8$ ) that shook the Sichuan region, China, on the May 12, 2008, caused significant cracks in the concrete slab of the 156 m-high Zippingku dam and, at least for several hours, some anxiety for the safety of the highly populated areas in the downstream region. The Zippingku Dam incident demonstrated very clearly the need to improve our basic understanding of the slab performance of CFRDs during strong earthquake shaking.

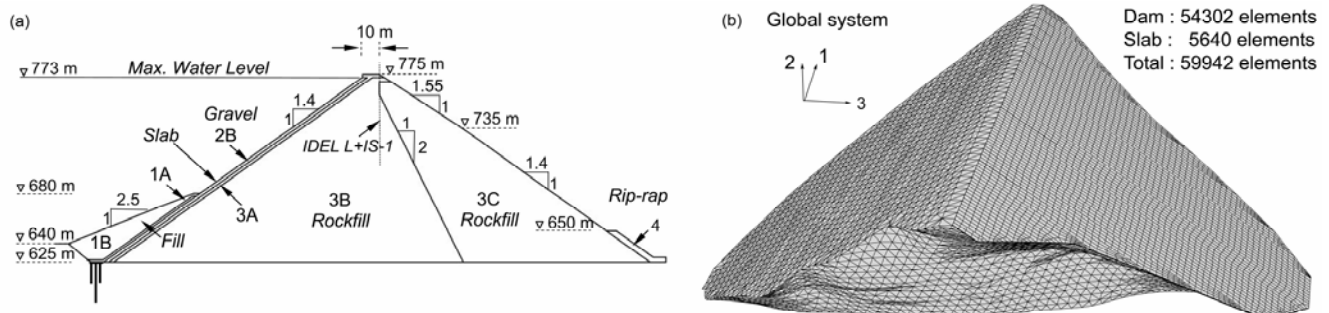


Figure 1. Messochora CFRD: (a) Maximum cross-section and material zones (b) 3D discretization of embankment and slab

The seismic performance of a CFRD depends on a large number of factors, such as the quality of compaction, the quality of rockfill, the dam geometry, the narrowness of the canyon, the irregularity of the abutment surface, the flexibility of the canyon rock, the quality of joints between adjacent slab panels and along the plinth, the ground motion intensity, characteristics and spatial variability, etc. (Gazetas & Dakoulas 1992, Dakoulas & Hsu 1995, Abouseeda & Dakoulas 1998). To be able to study the effect of such factors on the structural integrity of the entire face slab system, a realistic simulation of the phased construction and loading due to reservoir filling is an essential requirement.

The objective of this paper is to present a methodology for a realistic evaluation of the seismic behavior of the dam and slab, based on simulation of the phased construction, reservoir filling and earthquake shaking. The multi-stage static analysis is based on the Duncan et al. (1970) constitutive model, whereas the dynamic analysis uses on a nonlinear hysteretic model which accounts for the initial dynamic stiffness of the rockfill material. The model produces hysteresis loops that are in agreement with the experimental data regarding the variation of the shear modulus and damping ratio with cyclic shear strain. The Duncan model with the hysteretic formulation are implemented as a single “user material” in the finite element program ABAQUS (2008).

This paper presents the results of a very refined nonlinear 3-D analysis of Messochora CFRD, built in a narrow gorge of the Acheloos River in the north part of Greece. The dam has a height of 150 m at its maximum cross-section, a crest length of 350 m, and supports a 160 MW power station. The reservoir has a live storage volume of  $228 \cdot 10^6 \text{ m}^3$ . The geometry of the maximum cross-section of the dam and its material zones are shown in Fig. 1a. The upstream slope is 1:1.4, whereas the downstream slope is 1:1.4 at the lower 110 m and 1:1.55 at the upper 40 m. Zones 3B and 3C consist of rockfill obtained from quarries or necessary excavations, utilizing healthy or slightly weathered limestone. The material was compacted in four passes by a 12 ton vibratory roller, using a layer thickness equal to 100 cm for zone 3B and 150 cm for zone 3C. The average void ratio of the rockfill after compaction is 0.38. The concrete slab was placed upon a 4 m thick layer of well graded gravel (zone 2B), which due to its gradation and heavier compaction is quite stiffer than zone 3B. A zoned fill was placed upon the slab up to a height of 55 m from the dam base as an additional line of defense against seepage. Fig. 1b illustrates the discretization of the 3-D dam geometry, consisting of 54302 elements for the dam body and 5640 elements for the concrete slab.

## 2. DYNAMIC ANALYSIS

The numerical simulation is performed in eight stages:

- Stage 1:** The dam body is constructed in a sequence of 20 height increments.
- Stage 2:** The concrete slab is placed upon the upstream slope.
- Stage 3:** A fill is placed upon the slab from el. 625 m to an elevation of 680 m.
- Stage 4:** Additional settlements occur due to creep of the dam material.
- Stage 5:** The reservoir water is raised to an elevation of 680 m.
- Stage 6:** The reservoir water is raised to elevation of 725 m.
- Stage 7:** The reservoir water is raised to an elevation of 773 m.
- Stage 8:** The dam base is subject to earthquake shaking

A detailed description of the numerical formulation and the results of the phased construction and subsequent reservoir impoundment is given by Dakoulas et al. (2008). This paper presents representative results from the dynamic analysis.

### 2.1. Hysteretic model for rockfill

The shear modulus at small strains is given by

$$G_0 = 1000 A \frac{(2.17 - e)^2}{1 + e} (p'_0)^r \quad (1)$$

where  $p'_0$  = mean effective stress,  $e$  = void ratio,  $A$ ,  $r$  = material constants. During monotonic loading, the

hysteretic model assumes that the secant shear modulus is given by

$$G_s/G_0 = \frac{a}{1 + \exp(-(\log \gamma_e - c)/b)} \quad (2)$$

where  $a, b, c$  = material constants and  $\gamma_e$  = equivalent shear strain given by

$$\gamma_e = \sqrt{\frac{2}{3}} \sqrt{(\varepsilon_{11} - \varepsilon_{22})^2 + (\varepsilon_{22} - \varepsilon_{33})^2 + (\varepsilon_{33} - \varepsilon_{11})^2 + 3(\gamma_{12}^2 + \gamma_{23}^2 + \gamma_{31}^2)/2} \quad (3)$$

For the special case of  $\varepsilon_{11} = \varepsilon_{22} = \varepsilon_{33} = \gamma_{23} = \gamma_{13} = 0$ , eq. (1) yields that  $\gamma_e = \gamma_{12}$  and therefore the material constants  $a, b, c$  can be calibrated from experimental results on the variation of the shear modulus ratio and damping ratio versus the amplitude of cyclic shear strain. The tangent shear modulus for monotonic loading is given by

$$G_t/G_0 = \frac{a}{1 + \exp(-(\log \gamma_e - c)/b)} + \frac{a \exp(-(\log \gamma_e - c)/b)}{b (1 + \exp(-(\log \gamma_e - c)/b))^2 \ln 10} \quad (4)$$

whereas for unloading and reloading (based on the Masing criterion) it becomes

$$G_t/G_0 = \frac{a}{1 + \exp(-(\log(|\gamma - \gamma_{ref}|/2) - c)/b)} + \frac{a \exp(-(\log(|\gamma - \gamma_{ref}|/2) - c)/b)}{b (1 + \exp(-(\log(|\gamma - \gamma_{ref}|/2) - c)/b))^2 \ln 10} \quad (5)$$

where  $\gamma$  = deformation vector and  $\gamma_{ref}$  = the deformation vector from which unloading or reloading took place. Fig. 2 presents the mean value and one standard deviation of the shear modulus ratio  $G_s/G_0$  and damping ratio  $\xi$  versus the cyclic shear strain for gravel (Rollins et al. 1998). It also gives the values of  $G_s/G_0$  and  $\xi$  predicted by this hysteretic model for  $a = 1.014$ ,  $b = -0.65$  and  $c = -1.30$ . Fig. 3 presents the imposed simple shear deformation on a soil element and the stress-strain relationship derived from the hysteretic model.

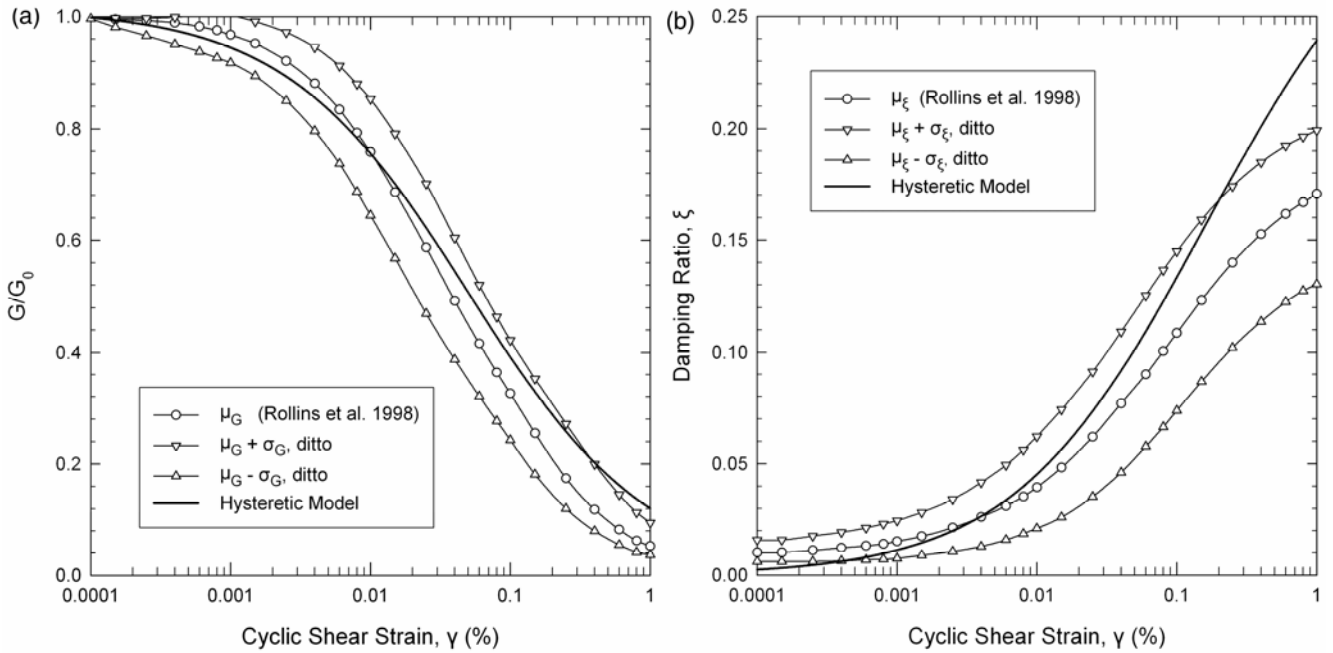


Figure 2. Dynamic properties of gravel from extensive experimental results (Rollins et al. 1998) and the hysteretic model: (a) secant shear modulus ratio,  $G_s/G_0$  (b) hysteretic damping ratio,  $\xi$ , vs cyclic shear strain.

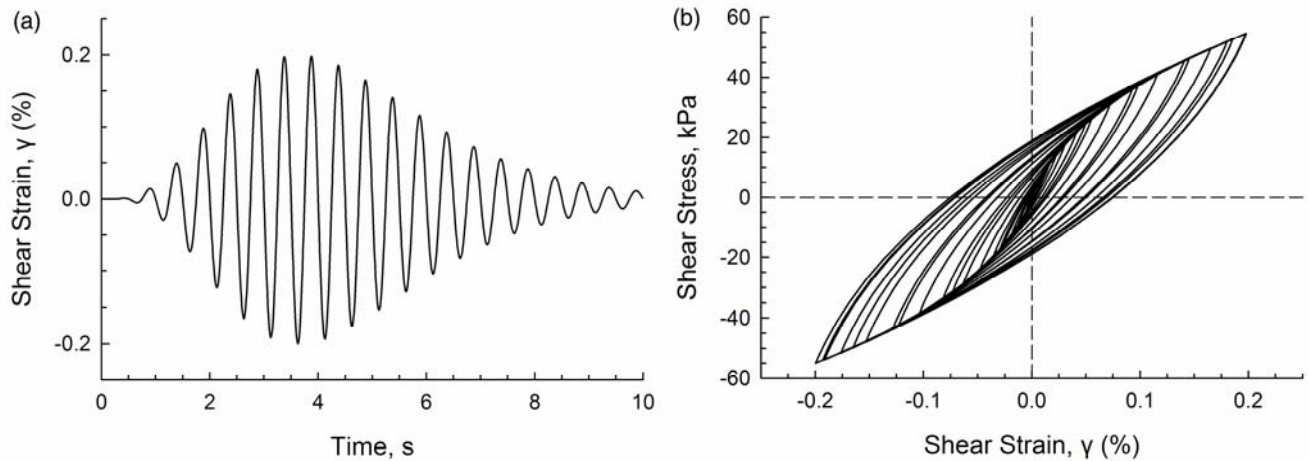


Figure 3. Simulation of a simple shear test using the hysteretic model: (a) imposed shear strain history (b) predicted stress-strain relationship.

Table 1. Properties and model parameters for gravel and rockfill

	Zone 3B	Zone 3C	Zone 2B
Density, $\rho$ , kg/m <sup>3</sup>	2150	2150	2150
Void ratio, $e$	0.38	0.38	0.30
Poisson's ratio, $\nu$	0.35	0.35	0.35
Duncan model parameters (Dakoulas et al. 2008)			
$K$	600	450	1200
$K_{ur}$	1500	1125	3000
$K_b$	150	112.5	300
$n$	0.45	0.45	0.45
$m$	0.22	0.22	0.22
$R_f$	0.59	0.59	0.59
$\phi_0$	51°	51°	51°
$\Delta\phi$	9°	9°	9°
Scenario A			
$A$	14300	10725	28600
$r$	0.5	0.5	0.5
Scenario B			
$A$	19000	14250	38000
$r$	0.5	0.5	0.5
Scenario C			
$A$	23500	17625	47000
$r$	0.5	0.5	0.5
Gravel-to-concrete friction coefficient, $\mu$		0.7	

Table 2. Properties of concrete

Density $\rho$ , kg/m <sup>3</sup>	2350
Young's Modulus, $E$ , GPa	21
Poisson's ratio, $\nu$	0.2
Concrete-to-concrete friction coefficient, $\mu_c$	0.5

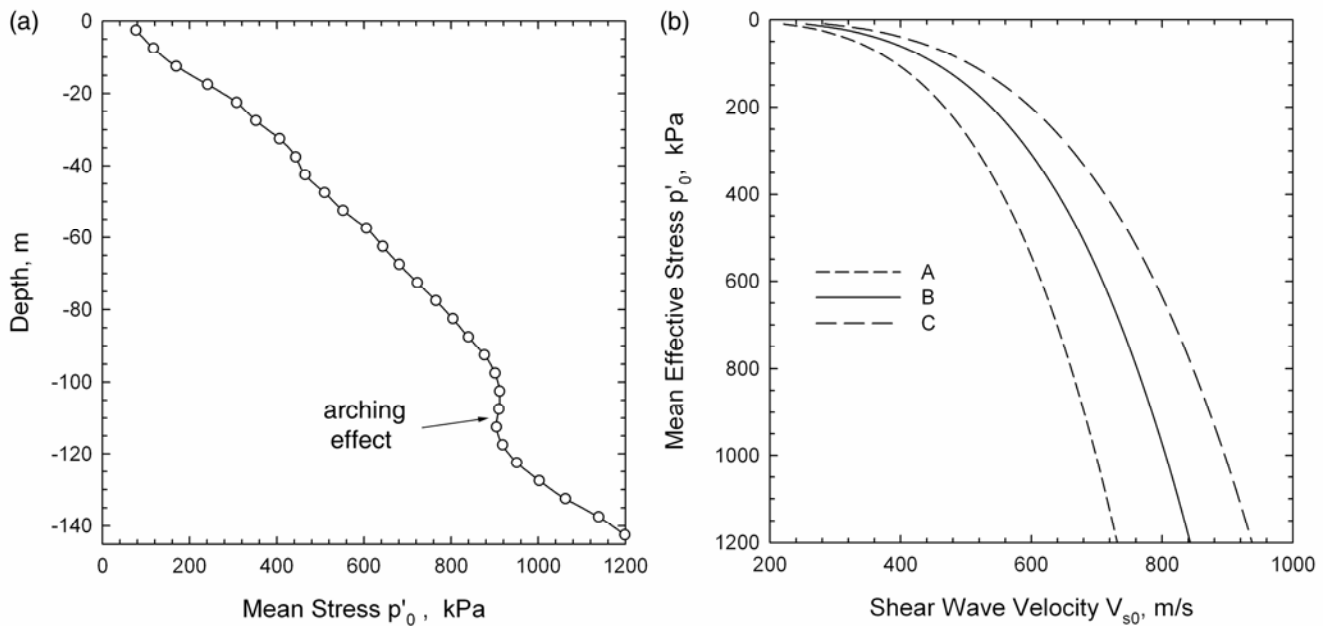


Figure 4. (a) Variation of the mean stress  $p'_0$  with depth from the crest at maximum cross-section (b) Shear wave velocity at small strains  $V_{s0}$  versus mean stress for the three stiffness cases examined.

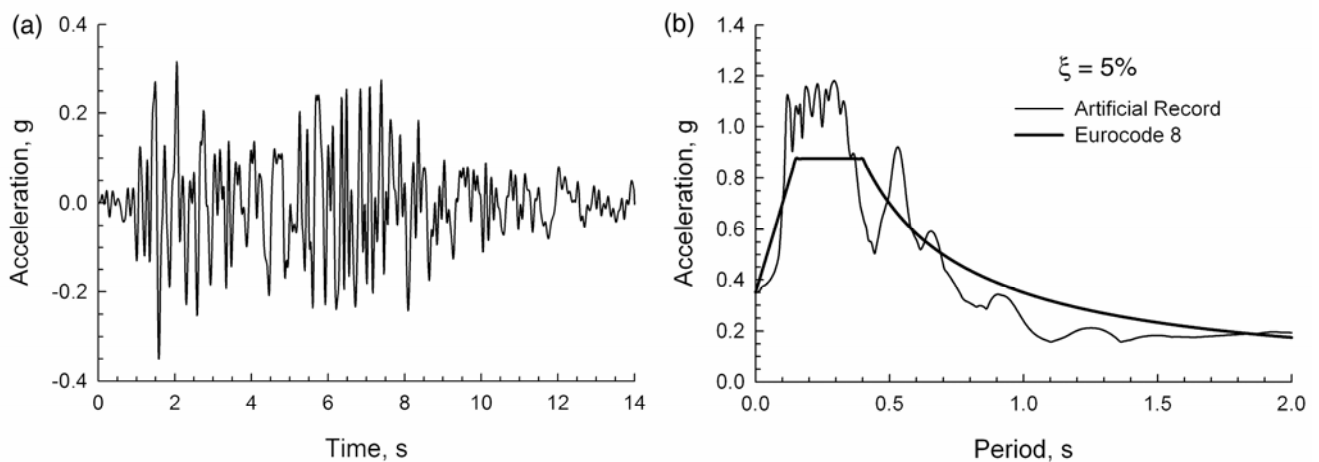


Figure 5. Seismic Excitation: (a) Acceleration time history (b) Acceleration spectra and Eurocode spectra for soil type A (rock and rock-like formations with  $V_{s30} \geq 800$  m/s).

### 2.2. Dynamic stiffness for rockfill

Due to the lack of in situ measurements, three cases are considered for the shear wave velocity at small strains computed from  $V_{s0} = \sqrt{G_0 / \rho}$ , where  $G_0$  = the shear modulus at small strains from eq. (1). Case A corresponds to a moderately stiff dam, Case B to a stiff dam and Case C to a very stiff dam. The material constants  $A$  and  $r$  for the three cases are given in Table 1. Fig. 4a plots the distribution of the mean stress  $p'_0$  versus depth from the crest, whereas Fig. 4(b) plots the variation of  $V_{s0}$  versus  $p'_0$  for the three scenarios. It is estimated that the true stiffness of the dam is between the values of scenarios A and B.

### 2.3. Earthquake excitation

This study considers that the design earthquake has a magnitude about  $M = 6.5$  and a peak ground acceleration of  $0.35g$ . It is caused by a normal fault with an epicentral distance about 5-10 km and a depth about 5-10 km. Several seismic excitations have been used in the course of this study based on historic and artificial records. However, due to lack of space, only one excitation is examined in this paper. Fig. 5 presents the acceleration time history and response spectra, as well as the Eurocode spectra for soil type A (rock and rock-like formations with  $V_{s30} \geq 800$  m/s). The excitation is exerted in the horizontal upstream-downstream direction.

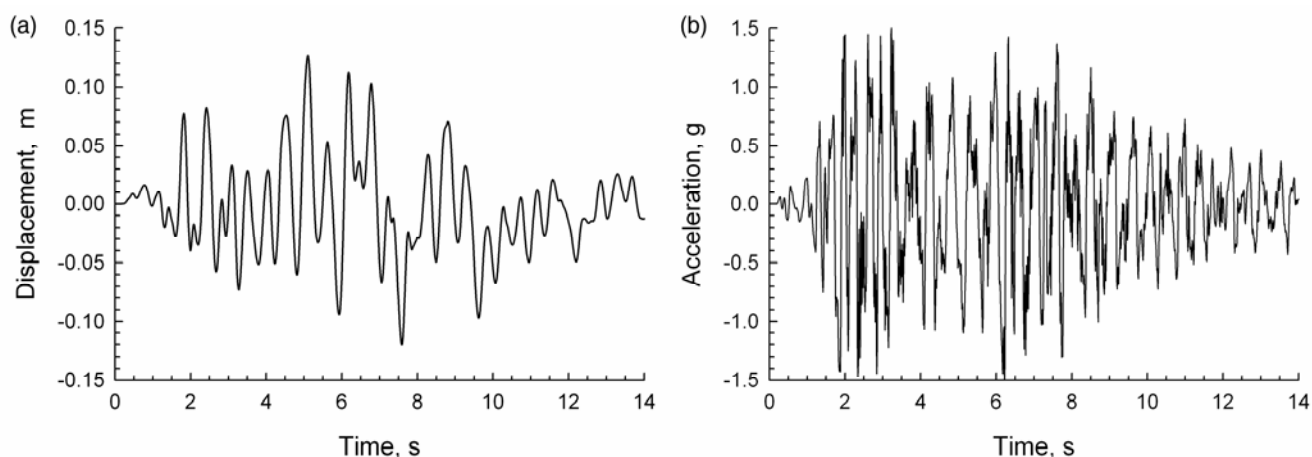


Figure 6. Case A: (a) Hor. displacement time history (b) Hor. acceleration time history at mid-crest.

### 3. RESULTS AND CONCLUSIONS

Fig. 6 presents the horizontal displacement and acceleration at mid-crest for Case A. The maximum displacement is  $\approx 0.13$  m and the maximum acceleration  $\approx 1.5g$ . The peak accelerations for the stiffer rockfill Cases B and C are 1.63g and 1.8g, respectively. Despite the very high magnitude, such peak accelerations, acting during a very short time, do not affect the stability of the dam. Results using other excitations based on historic records from rock sites yield mid-crest displacement between 0.10–0.15 m and peak accelerations between 1g–1.8g. Fig. 7a (left) plots tensile stresses within the slab with values  $>4$  MPa, which is an approximate limit for the development of tensile cracks, for Case A. These tensile stresses are slightly higher compared to those from the static analysis (Dakoulas et al. 2008) and are located in a zone about 30–50 m wide, parallel to the plinth at the lower 2/3 of the slab. As expected, by increasing the rockfill stiffness in Cases B and C, the magnitude of the tensile stresses decreases (Figs. 7b and 7c). Fig. 7a (right) plots the compressive stresses exceeding the value of -10 MPa, for Case A. The maximum compressive stresses do not exceed the compressive strength of concrete and are located in the central area at about 2/3 of the dam height. The results in Fig. 7 were computed without accounting for any dynamic compaction during shaking. A strong ground shaking may induce dynamic settlements, such as in the 85m-high Cogoti dam (Chile) during the 1943 Illapel earthquake ( $M=7.9$ ), in which the crest settled by 0.4 m. It is anticipated that a CFRD during a strong shaking may experience a maximum settlement about 0.5 to 1 m (Wieland 2007). Such settlements would impose additional deformations to the slab. To examine the effect of such a dynamic settlement on the slab, an analysis is conducted based on Case B, assuming a settlement of 0.5 m. Fig. 8a plots the maximum tensile and compressive stresses. Compared with the results in Fig. 7b, in which no settlement is considered, the results show that the settlement of 0.5 m leads to smaller tensile stresses but extends the zone of compressive stresses to a larger area that reaches to the crest. However, additional analyses have shown that settlements much higher than 0.5 m may increase the compressive stresses in this region to values exceeding the compressive concrete strength. Note that the results in Figs. 7 and 8 are taken from a large set of “snapshots” at various moments during shaking and that intermediate results may yield somewhat higher response. Fig. 8b plots the deflection  $U_z$  and the horizontal lateral displacement  $U_y$  (Y direction) of the slab panels. The mid-crest deflection  $U_z$  from 0.28 m before the shaking becomes 0.85 m after the shaking. Also, the maximum hor. displacement  $U_y$  from 0.07 cm before the shaking becomes 0.17 m after the shaking. The distribution of the panel movements is such so that no water leaks are expected at the joints between the slabs. Finally, the displacements of the slabs in the longitudinal (X) direction remain  $< 0.05$  m at all times and, therefore, no leakage is expected along the plinth joints, too.

The presented methodology for nonlinear 3D static/dynamic FE analysis of CFRDs offers a powerful, effective computational tool for the integrated simulation of the phased construction, creep settlements, reservoir impoundment, and seismic shaking of the dam with (or without) dynamic settlements. The method allows a detailed evaluation of the development of the tensile stresses within the concrete slab panels, of the compressive stresses at the slab-to-slab vertical interfaces and the behavior of the joints. Results of parametric studies for the improvement of our understanding of the seismic behavior of CFRDs will be published elsewhere.

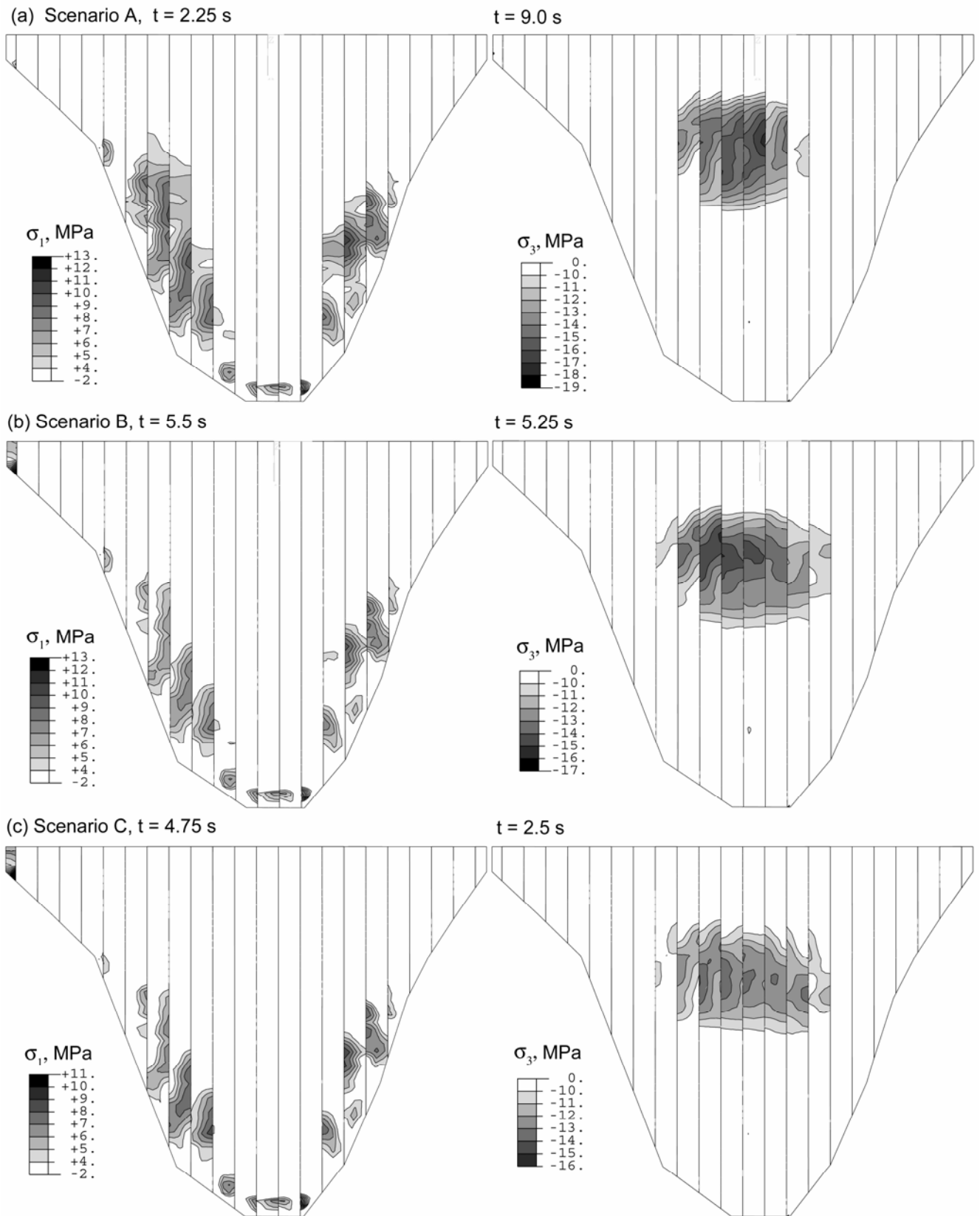


Figure 7. Distribution of the maximum tension (left) and maximum compression (right) in the slab during seismic shaking for a range of values of the rockfill stiffness: (a) Case A (b) Case B and (c) Case C.

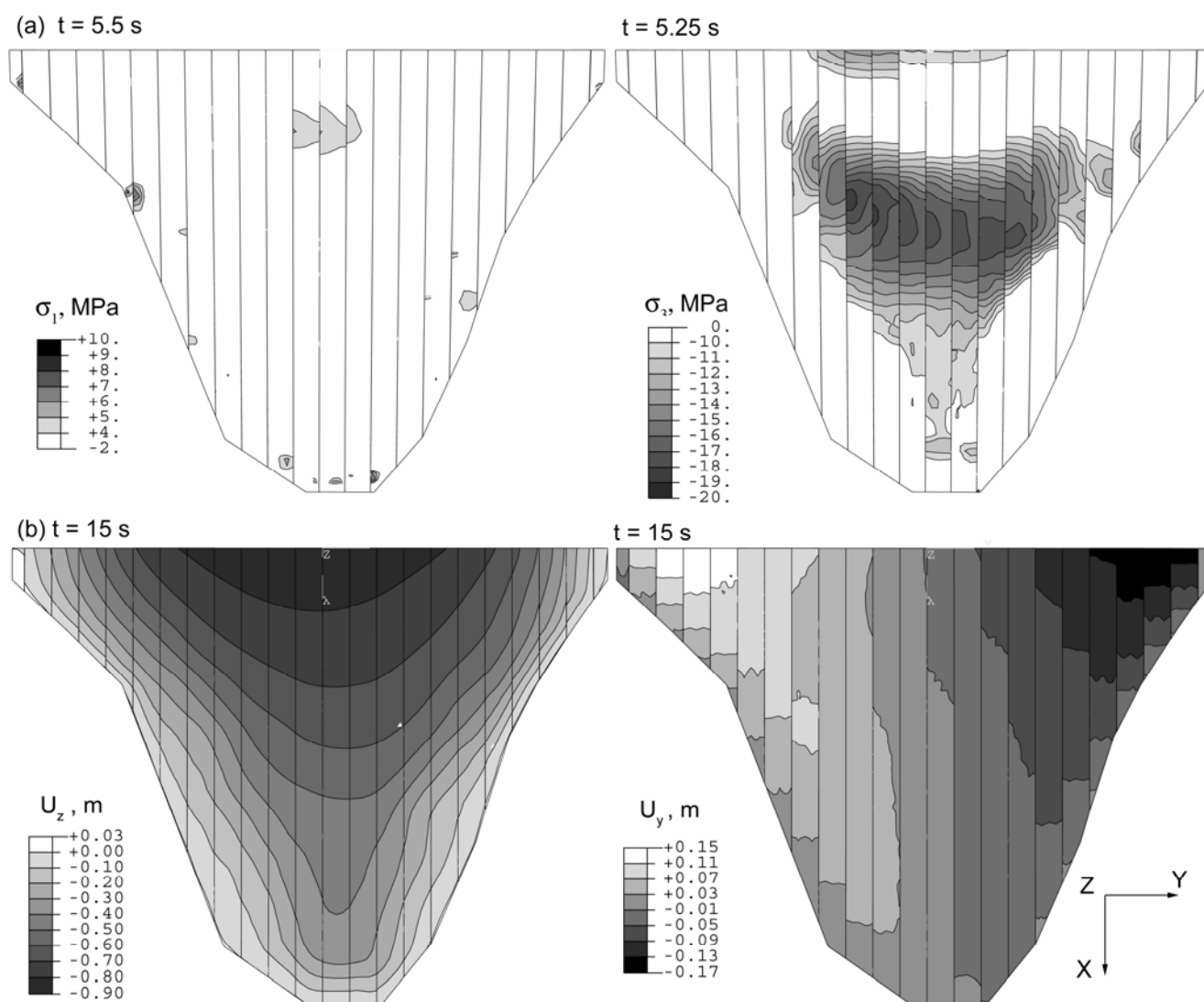


Figure 8. Case B with a 0.5 m dynamic settlement: (a) Maximum tension (left) and maximum compression (right) in the slab during shaking (b) Deflection and hor. lateral movement of the slab after the earthquake.

#### 4. REFERENCES

- ABAQUS (2008), *Users' Manual*, Version 6.7, Hibbit, Karlsson, and Sorenson, Inc., Pawtucket, Rhode Island.
- Abouseeda, H. and Dakoulas, P. (1998), Nonlinear Earth Dam - Foundation Interaction Using a BE-FE Method, *J. of Earthquake Engineering and Structural Dynamics*, Vol. 27(12), 917-936.
- Dakoulas, P., Thanopoulos, Y., and Anastassopoulos, K (2008), "Nonlinear 3D simulation of CFR dam construction and reservoir filling", *International Journal of Hydropower and Dams*, Issue 2, 95-101.
- Dakoulas, P., and Hsu (1995), "Response of Earth Dams in Semi-Elliptical Canyons to Oblique SH Waves", *Journal of Engineering Mechanics*, ASCE, Vol. 120, 3, pp. 379-391.
- Duncan J. M. and C. Y. Chang (1970). Nonlinear analysis of stress and strain in soils, *J. of Soil Mech. And Found. Engineering*, ASCE, 96(5), 1629-1653.
- Gazetas, G. and Dakoulas, P. (1992), "Seismic Analysis and Design of Rockfill Dams: State of the Art", *Journal of Soil Dynamics and Earthquake Engineering*, Vol. 11, No. 1, pp. 27-61.
- Rollins, K., Evans, M., Diehl, N.B., Daily, W.D. (1998), Shear modulus and damping relations for gravel, *J. Geotechn. and Geoenvironm. Engineering*, ASCE, 124(5), 396-405
- Sherard, J.L. & Cooke, J.B. (1987), Concrete face rockfill dams: Assessment. *J. Geotechnical Engineering*, ASCE, 113(10), 1096-1112.
- Wieland, M. (2007), Seismic Performance of CFRDs, *Water Power and Dam Construction*, March.